Effect of oligothiophene π-bridge length in D-π-A star-shaped small molecules on properties and photovoltaic performance in single-component and bulk heterojunction organic solar cells and photodetectors

Luponosov, Yuriy N.; Solodukhin, Alexander N.; Mannanov, Artur L.; Savchenko, Petr S.; Raul, Benedito A.L.; Peregudova, Svetlana M.; Surin, Nikolay M.; Bakirov, Artem V.; Shcherbina, Maxim A.; Chvalun, Sergei N.

Published in:
Materials Today Energy

DOI:
10.1016/j.mtener.2021.100863

Publication date:
2021

Materials Today Energy 22 (2021) 100863

Contents lists available at ScienceDirect

Materials Today Energy

journal homepage: www.journals.elsevier.com/materials-today-energy/

Effect of oligothiophene π-bridge length in D-π-A star-shaped small molecules on properties and photovoltaic performance in single-component and bulk heterojunction organic solar cells and photodetectors

Yuriy N. Luponosov [a, *, g], Alexander N. Solodukhin [a, g], Artur L. Mannanov [a, b], Petr S. Savchenko [a], Benedito A.L. Raul [c], Svetlana M. Peregudova [a, d], Nikolay M. Surin [a], Artem V. Bakirov [a, e], Maxim A. Shcherbina [a, f], Sergei N. Chvalun [a, e], Maxim S. Pshenichnikov [c, **], Dmitry Yu Paraschuk [a, b, ***], Sergey A. Ponomarenko [a]

[a] Enikolopov Institute of Synthetic Polymeric Materials of the Russian Academy of Sciences, Profsoyuznaya st. 70, Moscow, 117393, Russia
[b] Faculty of Physics, Lomonosov Moscow State University, Leninskie Gory 1/62, Moscow, 119991, Russia
[c] Zernike Institute for Advanced Materials, University of Groningen, Nijenborgh 4, 9747 AG, Groningen, the Netherlands
[d] Nesmeyanov Institute of Organoelement Compounds, Russian Academy of Sciences, Vavilova St. 28, Moscow, 119991, Russia
[e] National Research Center "Kurchatov Institute", Kurchatov sq. 1, Moscow, 123182, Russia
[f] Moscow Institute of Physics and Technology, 9 Institutsky line, Dolgoprudny, Moscow region, 141701, Russian Federation

ARTICLE INFO

Article history:
Received 31 August 2021
Accepted 16 September 2021
Available online 23 September 2021

Keywords:
Donor-acceptor triarylamines
Intramolecular charge transfer
Exciton diffusion
Photoluminescence
Ultrafast spectroscopy
Alkyl dicyanovinyl group

ABSTRACT

Donor-acceptor molecules with thiophene fragments as the π-bridge represent a promising class of materials for organic photovoltaics especially in single-component (SC) organic solar cells (OSCs) and other related applications. However, the effect of the oligothiophene π-bridge length on physicochemical properties, photophysics, charge transport, and photovoltaic performance of these materials has not been thoroughly addressed. Here, we report on the synthesis and comprehensive investigation of the series of star-shaped donor-acceptor molecules (**0T**–**4T**) with triphenylamine as a donor core linked through an oligothiophene π-bridge of variable length to the terminal hexyl-dicyanovinyl electron-withdrawing groups. We found that variation of the π-bridge length from 0 to 4 thiophene units strongly impacts their properties such as the solubility, highest occupied molecular orbital energy, optical absorption and photophysics, film morphology, phase behavior, and molecular packing as well as the charge carrier mobility. The performance of the SC and bulk heterojunction OSCs and photodetectors is comprehensively studied and compared. The results obtained provide insight into how to fine-tune and predict properties and photovoltaic performance of small molecules for organic solar cells and photodetectors.

1. Introduction

Organic solar cells (OSCs) have been showing significant increase in efficiency in recent years achieving power conversion efficiency (PCE) of more than 18% in non-fullerene bulk heterojunction (BHJ) devices [1–3]. Single-component (SC) OSCs have attracted a lot of attention from the organic photovoltaics community owing to several crucial benefits, including simple resulting device structure and the lack of active layer morphology segregation [4–9]. Recently, it has been shown that utilization in SC OSCs, a photoactive layer based on molecules with a rather sophisticated so-called 'double cable' molecular architecture in which small-molecule acceptor fragments are linked covalently but without π-conjugation to the donor polymer backbone, allows achieving remarkable PCE more than 8% [10]. Although the PCE of SC OSC based on simple conjugated small molecules lags behind, it has also reached remarkable 2.9% [11].

* Corresponding author.
** Corresponding author.
*** Corresponding author.
E-mail addresses: luponosov@ispm.ru (Y.N. Luponosov), m.s.pchenitchnikov@rug.nl (M.S. Pshenichnikov), paras@physics.msu.ru (D.Y. Paraschuk).
[g] Yu. N. Luponosov and A. N. Solodukhin contributed equally to this work.

https://doi.org/10.1016/j.mtener.2021.100863
2468-6069/

Donor-acceptor (D-A) conjugated small molecules are one of the most promising organic architectures for use in both BHJ and SC OSCs [12–16]. Small molecules have several advantages compared with polymers: a clearly defined chemical structure, easy purification, and as a result, the high reproducibility in the output parameters of optoelectronic devices based on them. Optimization and fine-tuning of properties of D-A molecules are one of the most important tasks to be solved to improve the characteristics and stability of optoelectronic devices based on them. Variation of the electron donor and electron-withdrawing groups as well as the type and length of the conjugated π-bridge between them allows adjusting the energies of the highest occupied molecular orbital (HOMO) and lowest unoccupied molecular orbital (LUMO), bandgap (E_g), absorption and luminescence spectra, phase behavior, photophysics, and charge separation [13,17–21]. Oligothiophene fragments are one of the most frequently used π-conjugated bridges in the design of D-π-A systems [22–30]. Methods for controlling the electronic and optical properties of linear D-π-A systems by increasing the length of π-bridge have been described in the literature [31–35]. Importantly, it is natural to expect that the π-bridge length in D-π-A systems controls the extent of intramolecular photoinduced electron-hole separation, which results in a charge-transfer state — a precursor for photoinduced-free charges in OSCs.

The star-shaped architecture in design of D-A small molecules brings a number of advantages over the linear architecture [18,36–38]. Star-shaped D-A organic molecules based on the triphenylamine (TPA) core possess promising properties such as high stability and hole mobility, good solubility in organic solvents [13,19,39,40]. Roncali et al. [41,42] published pioneering works on synthesis and OSC application of star-shaped D-A small molecules based on the TPA donor core linked through monothiophene and bithiophene bridges to terminal dicyanovinyl electron-withdrawing groups. To the best of our knowledge, only a few investigations of the oligothiophene π-bridge length effect on the properties and photovoltaic performance of D-A star-shaped molecules were reported, specifically on the limited series of molecules usually by comparing the two or three nearest homologs [43,44]. Moreover, the performance of SC OSCs and the very possibility of SC OSC-based photodetectors have not yet been addressed.

In this work, we report on the synthesis of the series of TPA-based star-shaped molecules end-capped with hexyl-dicyanovinyl electron-withdrawing groups and having different lengths of the π-conjugated oligothiophene bridge, from 0 to 4 thiophenes (Fig. 1). All the molecules demonstrated small voltage losses in the SC OSCs resulting in high open-circuit voltage of 1.03–1.14 V. The PCE jumped from 0.06% for **1T** to the remarkable 1.09% for **4T** with π-bridge elongation, which is in a good agreement with their charge transport, generation, and recombination properties, as supported by the ultrafast photoluminescence (PL) spectroscopy, Onsager model calculations, and space-charge-limited current measurements. We also studied SC OSCs as photodetectors. The photovoltaic performance in

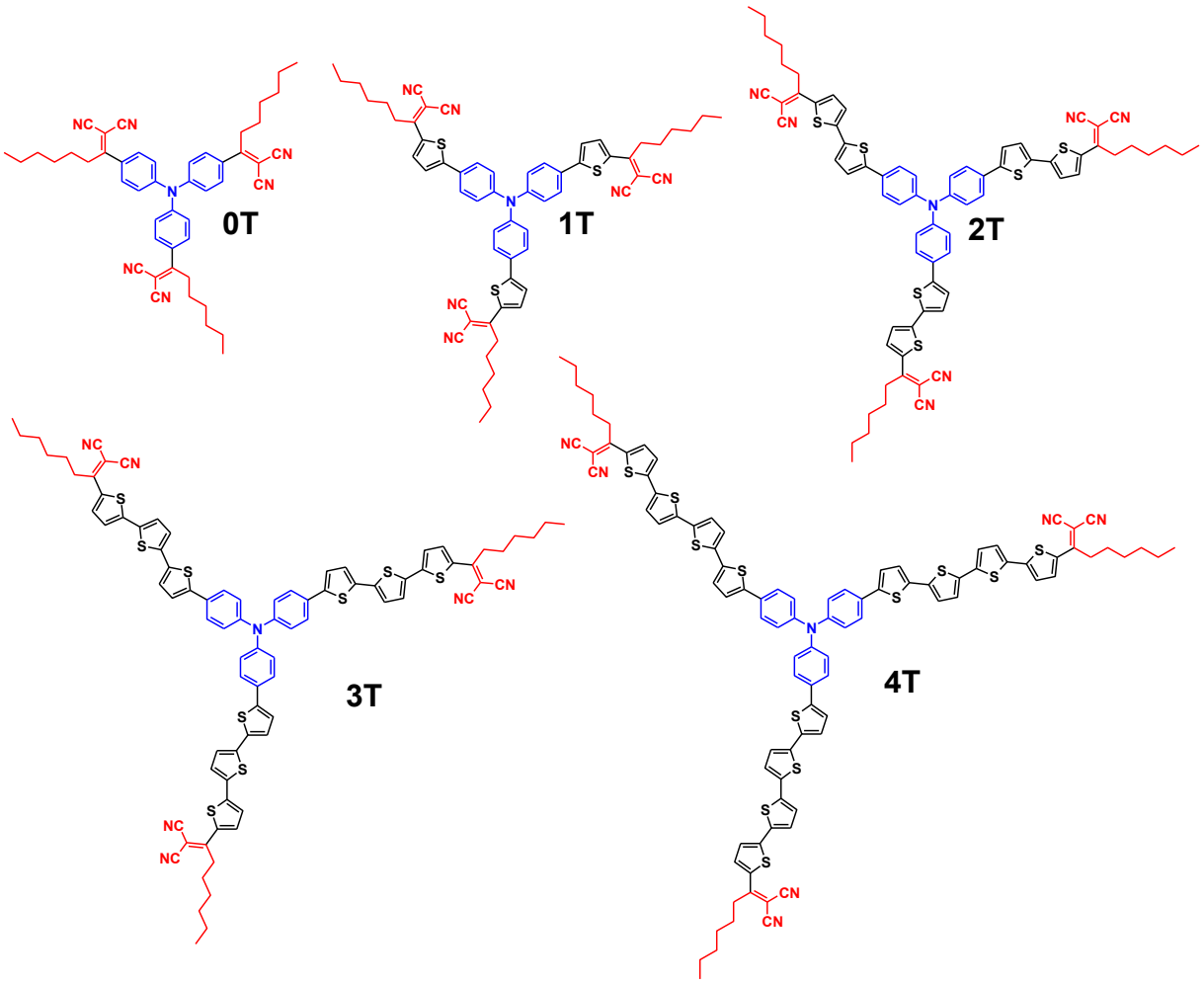

Fig. 1. Chemical structures of the star-shaped D-π-A molecules **0T**, **1T**, **2T**, **3T** **4T**.

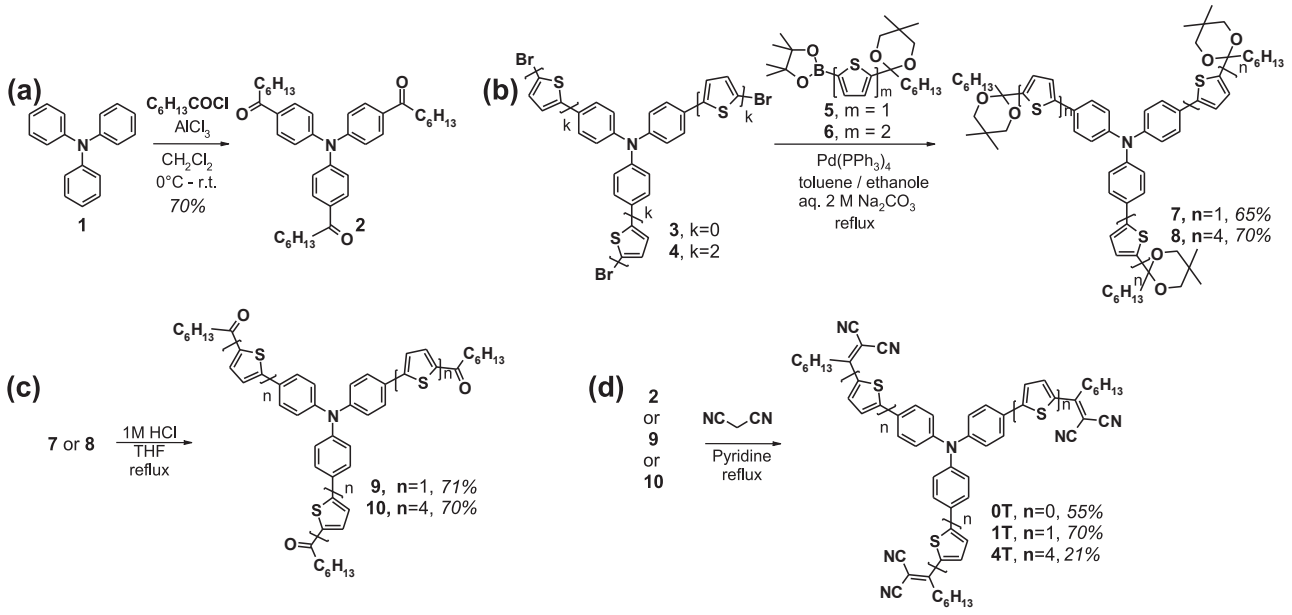

Fig. 2. Synthetic scheme of **0T**, **1T**, **4T**.

BHJ OSCs with $PC_{71}BM$ as the acceptor increased significantly with elongation of the π-bridge length from **0T** to **2T** mainly because of the improved sunlight absorption and film morphology. However, the further absorption redshift and increase in performance of BHJ OSCs with elongation of the oligothiophene length were hampered by the decrease in the intramolecular charge transfer efficiency and the exciton diffusion length.

2. Results and discussion

2.1. Synthesis

The synthesis of **2T** and **3T** molecules has been reported previously [44,45], whereas the preparation of novel **0T**, **1T,** and **4T** molecules is depicted in Fig. 2. The synthesis of model compound **0T** was carried out in two steps. First 1,1′,1″-[nitrilotris(4,1-phenylene)]triheptan-1-one (**2**) was prepared in 70% yield by Friedel-Crafts acylation of TPA (**1**) with heptanoyl chloride in the presence of aluminum chloride (Fig. 2a). Then **0T** was prepared by Knoevenagel condensation of the ketone (**2**) with malononitrile in the pyridine solution under microwave heating (Fig. 2d).

The key step for the synthesis of **1T** and **4T** molecules was Suzuki cross-coupling reaction between the corresponding brominated TPA core (**3** or **4**) and ketal (**5** or **6**) (Fig. 2 b). Thus, *tris*{4-[5-(2-hexyl-5,5-dimethyl-1,3-dioxan-2-yl)-2-thienyl]phenyl}amine (**7**) was prepared in 65% yield by cross-coupling reaction between *tris*(4-bromophenyl)amine (**3**) and 2-hexyl-5,5-dimethyl-2-[5-(4,4,5,5-tetramethyl-1,3,2-dioxaborolan-2-yl)-2-thienyl]-1,3-dioxane (**5**) under Suzuki conditions. *Tris*{4-[5‴-(2-hexyl-5,5-dimethyl-1,3-dioxan-2-yl)-2,2′:5′,2″:5″,2‴-quatrothien-5-yl]phenyl}amine (**8**) was synthesized similarly by the reaction between bithiophene-containing *tris*[4-(5′-bromo-2,2′-bitien-5-yl)phenyl]amine (**4**) and 2-hexyl-5,5-dimethyl-2-[5'-(4,4,5,5-tetramethyl-1,3,2-dioxaborolan-2-yl)-2,2′-bithien-5-yl]-1,3-dioxane (**6**) in 70% yield.

On the next step, the protective 5,5-dimethyl-1,3-dioxane groups were removed by reflux of ketals **7** and **8** in tetrahydrofuran (THF) with 1 M HCl to give trifunctional ketones 1,1′,1''-[nitrilotris (4,1-phenylenethiene-5,2-diyl)]triheptan-1-one (**9**) and *tris*{4-[5‴-(2-hexyl-5,5-dimethyl-1,3-dioxan-2-yl)-2,2′:5′,2'':5″,2‴-quaterthien-5-yl]phenyl}amine (**10**) in 71% and 70% yield, respectively (Fig. 2c).

The target *tris*[4-(1,1-dicyanooct-1-en-2-yl)phenyl]amine (**0T**), *tris*{4-[5-(1,1-dicyanooct-1-en-2-yl)-2-thienyl]phenyl}amine (**1T**), and *tris*{4-[5‴-(1,1-dicyanooct-1-en-2-yl)-2,2′:5′,2″:5″,2‴-quaterthien-5-yl]phenyl}amine (**4T**) were obtained in 55%, 70%, and 21% yields by Knoevenagel condensation between corresponding ketones (**2**, **9**, **10**) with malononitrile in the pyridine solution under a microwave heating (Fig. 2d). The low yield of **4T** is caused by losses during column chromatography purification because of its low solubility in chloroform which was used as the eluent. The chemical structure and high purity of the target products were confirmed by the complex of methods (see Experimental Part in Electronic Supplementary Information (ESI), Fig. S2.1-S2.10).

2.2. Solubility and thermal properties

0T, **1T**, **2T**, **3T** exhibited good solubility in low-polarity solvents such as THF, methylene chloride, chloroform, and *o*-dichlorobenzene (ODCB). In contrast, **4T** was poorly soluble in those organic

Table 1
Solubility and thermal properties of **0T**–**4T**.

Compound	Solubility[a], gL^{-1}	T_g, °C	ΔC_p, $Jg^{-1}K^{-1}$	T_m, °C	ΔH_m, Jg^{-1}	T_d (air/N_2), °C
0T	220	14	0.35	100	47	305/342
1T	88	54	0.23	–	–	355/393
2T	20	64	0.25	–	–	371/403
3T	12	72	0.29	–	–	388/388
4T	1	94	0.28	141	14	395/386

Notes: [a]in ODCB, T_g is the glass transition temperature of the second heating DSC, ΔC_p is the jump of heat capacity at T_g, T_m is the melting temperature, ΔH_m is the melting enthalpy, and T_d is the decomposition temperatures corresponding to 5% of the weight loss.

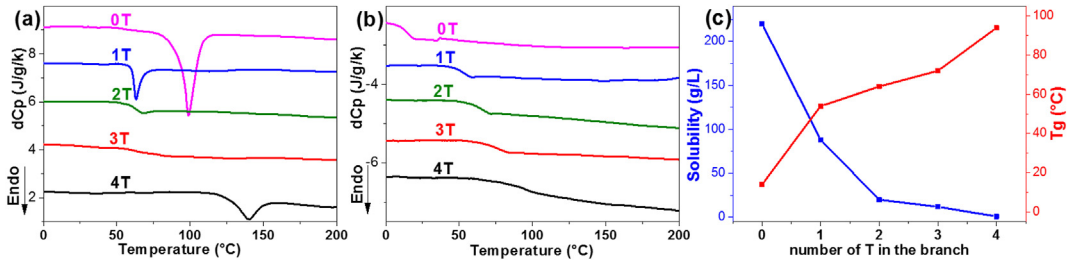

Fig. 3. The first (**a**) and second (**b**) DSC heating scans of **0T**–**4T**; (**b**) dependence of the solubility and T_g values on the oligothiophene π-bridge length.

solvents. The measured solubility values for the studied star-shaped D-A molecules in ODCB at room temperature showed a typical dependence for oligothiophenes: a decrease in solubility with increase of the oligothiophene π-bridge length (Table 1). The increase of the π-bridge length from 3 to 4 thiophene units led to a sharp drop in the solubility from 12 to 1 gL^{-1}.

Analysis of thermal and thermooxidative stability by the method of thermogravimetric analysis showed that all the 0T–4T materials have high thermal stability both in air and under inert atmosphere with the decomposition temperature exceeding 300 °C (see curves and discussion in ESI, Fig. S3.1 and Table 1).

Fig. 3 shows differential scanning calorimetry (DSC) scans for **0T**–**4T** molecules. **0T** and **4T** were found to be crystalline with melting temperatures (T_m) of 100 °C and 141 °C and the melting enthalpies (ΔH_m) of 47 Jg^{-1} and 14 Jg^{-1}, respectively (Fig. 3, Table 1). At the same time, only bending of the baseline on the DSC curves corresponding to the glass transition process is observed for **1T**, **2T,** and **3T** molecules. The presence of the endothermic peak at 63 °C on the first DSC heating scan of **1T** (Fig. 3a) is owing to a molecular relaxation phenomenon [46], because the glass transition occurs at the same temperature region as revealed by the second DSC heating scan (Fig. 3b). It should be noted that the endothermic effects were not observed on the DSC scan of the second heating for all materials. It is interesting to note that with the oligothiophene π-bridge elongation the glass transition temperature (T_g) increases opposite to the decrease of solubility (Fig. 3c). As anticipated, the higher the molecular weight of the molecules and the stronger intermolecular interactions, the higher T_g of the material and the lower solubility. DSC data agree well with the X-ray structural data (see ESI Section 3 and discussion therein).

2.3. Optical and electrochemical properties

Fig. 4 summarizes optical absorption data for **0T-4T**. As follows from the ultraviolet–visible (UV-vis) absorption spectra of **0T**–**4T** in diluted THF solutions (Fig. S4.1 and Table S4.1), elongation of the π-conjugated bridge leads to an increase in the molar extinction coefficient from 42,000 (**0T**) to 149,000 (**4T**) $M^{-1}cm^{-1}$ in the absorption maximum. The absorption spectra of **0T**–**4T** in solutions have similar shapes (Fig. 4a). Two types of absorption bands are observed: the bands in the region of 4.5–3.0 eV are attributed to the $\pi-\pi^*$ transition in the conjugated phenylene-oligothiophene fragment; and the intense bands in the long-wavelength region (3.1–2.07 eV) are attributed to intramolecular charge transfer (ICT) between the electron-donating TPA and electron-withdrawing dicyanovinyl blocks [47,48] or to a mixed character [19]. The red shift of the absorption maxima in solutions is pronounced with increase of the oligothiophene length from **0T** to **2T** and much less pronounced from **2T** to **3T**. And finally, a slight (a few nanometers) blue shift of the absorption maxima is observed with increase of nT from 3 to 4. This feature can be explained by the following. On the one hand, the 4T fragment the longest within this series of molecules — may lead to a rather intense and red-shifted π–π* transition band [49] overlapping partly with the ICT band. On the other hand, with elongation of the nT, the following two factors operate: (i) the number of torsion angles between thiophenes increases making non-planar and hence less conjugated conformations of nT more probable [50–52]; (ii) the distance between the central donor and terminal acceptor blocks increases. As a result, these (i-ii) factors can decrease the ICT efficiency and lead to a blue shift of the corresponding ICT band [53,54].

As follows from Fig. 4a and b, the absorption spectra in films are broadened, and their maxima are red-shifted by 0.09–0.24 eV in comparison with the spectra in solutions. Note a pronounced redshift of 0.24 eV for the **4T** absorption spectrum. It can be explained by the stronger ability of **4T** molecules to aggregate in the solid phase, which is in a good agreement with the solubility, phase behavior, and X-ray data (see above).

Fig. 5 presents PL spectra and PL quantum yield (PLQY) of **nT** molecules in diluted polymer (Paraloid B72) solutions. The redshift of the PL spectra from **0T** to **4T** is in a good agreement with their optical bandgap. The PLQY increases from 9% to 37% with the

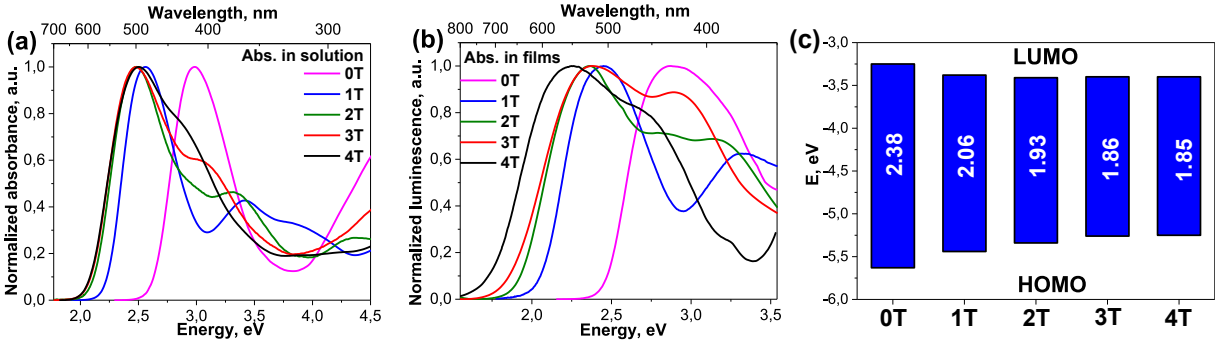

Fig. 4. UV–vis absorption spectra of **0T**–**4T** in THF solution (**a**) and film cast from THF solution (**b**) frontier orbital energies (as estimated from the CV data) of **0T**–**4T** (**c**).

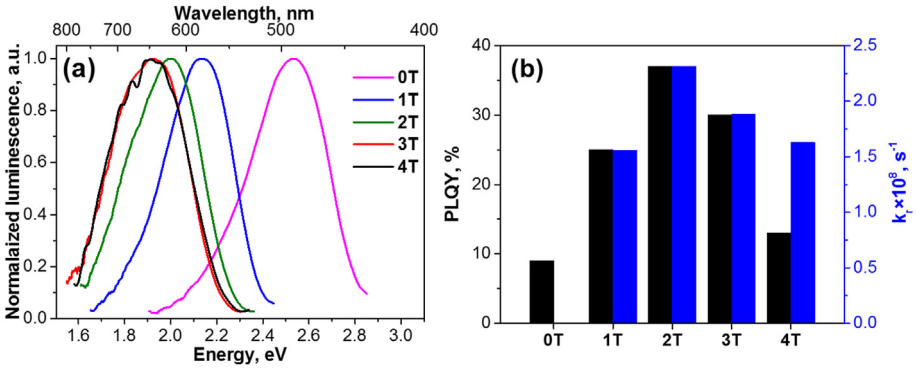

Fig. 5. Photoluminescence spectra of **0T**–**4T** in the polymer matrix (Paraloid B72) (**a**). PLQY and the radiative rate for **0T-4T.** (**b**). The radiative rates were calculated as $k_r = \mathrm{PLQY}/\tau$, where τ is the excited-state lifetime from Table 4.

elongation of the π-bridge length from **0T** to **2T** but then decreased down to 13% for **4T** (Fig. 5b). This bell-shaped dependence of PLQY closely follows the radiative rate for **1T**–**3T** extracted from the transient PL data presented in Section 2.4.3. However, PLQY drops essentially stronger than the corresponding radiation rate for **4T**. We assign this drop to more prominent non-radiative relaxation because to higher torsional floppiness of the long nT bridge. In addition, we cannot exclude aggregation of **4T** molecules during preparation and drying of their solid solutions as this molecule has much lower solubility (Table 1). This aggregation may also enhance non-radiative relaxation decreasing PLQY (Fig. 5b).

Note that the radiative rates calculated from the molar extinction and PL data (Fig. 5a and S4.1, Table S4.1) with the use of the Strickler-Berg relation [55,56] (Table S4.2) considerably overestimate the measured ones. As this relation is valid only for an isolated electronic transition, the obtained overestimation indicates that the lowest energy absorption band in the star-shaped oligomers corresponds not only to the single transition between the HOMO and LUMO but also to a set of transitions involving the almost degenerated orbitals located as well below the HOMO (HOMO−1, HOMO−2, and so on) and above the LUMO (LUMO+1, LUMO+2, and so on). In fact, this quasidegeneracy follows from the density functional theory (DFT) calculations reported for the star-shaped oligomers [57].

The electrochemical properties of the molecules were investigated by cyclic voltammetry (CV). The HOMO and LUMO energies

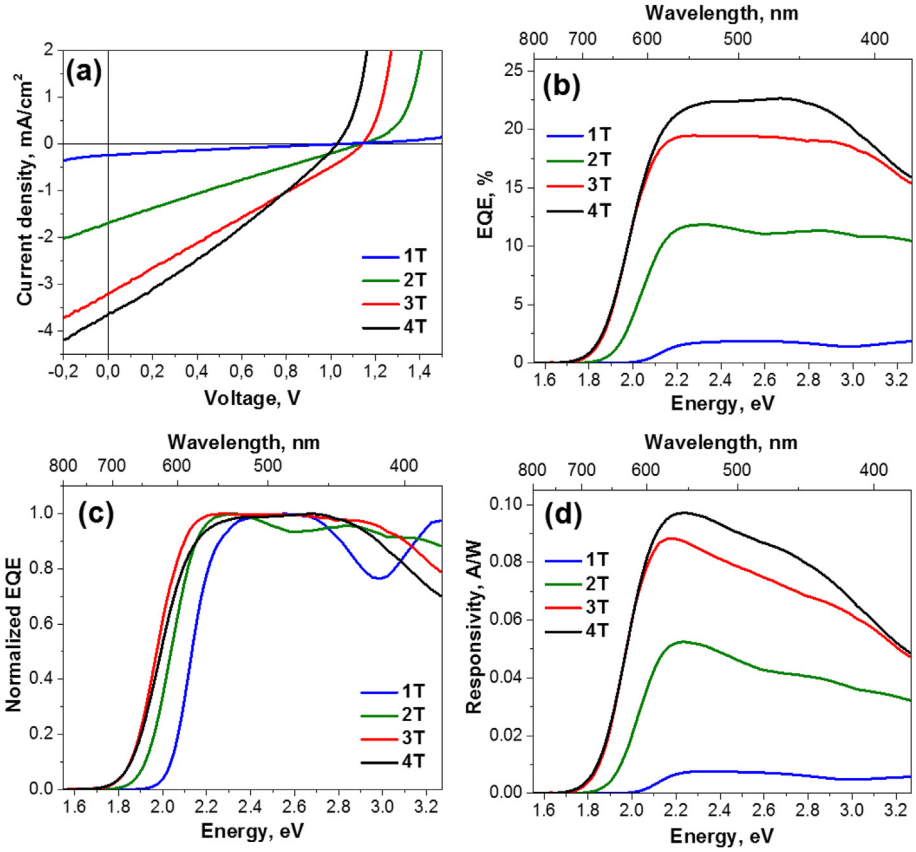

Fig. 6. *J-V* curves under AM1.5G illumination (100 mW/cm^2) (**a**) EQE spectra, (**b**) normalized EQE spectra, and (**c**) responsivity spectra (**d**) for SC OSCs.

Table 2
Hole (μ_h) and electron (μ_e) mobilities in **0T**–**4T** films.

Material	μ_h, $cm^2V^{-1}s^{-1}$	μ_e, $cm^2V^{-1}s^{-1}$	μ_h/μ_e
0T	$(1.09 \pm 0.28)\cdot10^{-6}$	-[a]	-[a]
1T	$(2.9 \pm 0.7)\cdot10^{-5}$	$(1.91 \pm 0.29)\cdot10^{-5}$	1.5
2T	$(1.5 \pm 0.4)\cdot10^{-4}$	$(1.15 \pm 0.12)\cdot10^{-5}$	13
3T	$(5.7 \pm 1.9)\cdot10^{-5}$	$(1.9 \pm 0.4)\cdot10^{-5}$	3
4T	$(4.6 \pm 1.5)\cdot10^{-5}$	$(3.0 \pm 0.6)\cdot10^{-5}$	1.5

Note: [a] We could not detect electron transport in the **0T** film by the SCLC method.

were calculated by using the first standard formal oxidation and reduction potentials (Fig. 4c and Table S4.1). We found that the introduction of the oligothiophene π-bridge and its following elongation leads to the significant increase of the HOMO energies from −5.63 to −5.25 eV. The LUMO energies were found to be significantly lowered from −3.25 to −3.40 eV with inclusion of the first thiophene unit, whereas no significant impact of further π-bridge elongation was observed. The latter can be explained by the fact that the electrochemical reduction proceeds mainly on the terminal alkyl-dicyanovinyl fragment [39,44], the local environment of which does not change significantly with the oligothiophene π-bridge elongation. Thus, the electrochemical bandgap within **0T**–**4T** series of molecules decreases from 2.38 eV to 1.85 eV, which is in a good agreement with the optical absorption data (Table S4.1).

2.4. Photovoltaic, charge transport, and photophysical properties

2.4.1. SC OSCs and photodetectors

Our recent investigation has revealed that D-A star-shaped molecules demonstrate promising performance in SC OSCs [20,57]. In this section, we address the effect of the oligothiophene π-bridge length in the series of **0T**–**4T** molecules on charge transport and photovoltaic properties in SC OSCs and photodetectors.

Because the device's active layer consists of only one material, its hole and electron mobilities should be comparable to ensure balanced charge transport of the photogenerated charges to the device electrodes after exciton dissociation in the bulk of the active layer. The hole and electron mobilities in films were measured by space-charge-limited current technique (for details see Section 1.4, ESI) presented in Table 2 (*J-V* characteristics of the hole and electron only devices are presented in Figs. S5.1–S5.9).

The close values of the hole and electron mobilities should be beneficial for SC OSCs to avoid space charge effects. Low or unbalanced charge mobility values can result in reduced device performance. The most balanced transport of holes and electrons was demonstrated by **1T**, **3T,** and **4T**. The **2T** showed the best hole transport, and the **4T** showed the best electron transport. The absence of electron transport in the **0T** indicates that this material is inappropriate for efficient SC OSCs.

To understand whether the differences in the charge mobility values are caused by different morphologies of the corresponding films, we performed the atomic force microscopy (AFM) study for the films (Fig. S5.14). The AFM data demonstrated smooth surfaces with indistinguishable morphologies and the root-mean-squared roughness of 0.32–0.34 nm.

Table 4
Excited-state lifetimes, efficiencies of formation of intermolecular CT excitons, and exciton diffusion lengths.

		1T	2T	3T	4T
Matrix	τ, ps	1600	1600	1600	800
Neat film	τ_1 (a_1), ps	200 (0.6)	40 (0.65)	15 (0.72)	10 (0.87)
	τ_2 (a_2), ps	1600 (0.4)	830 (0.35)	280 (0.28)	250 (0.13)
	τ_{avg}, ps	1400	770	250	200
	Q_{CTE}, %	13	50	85	75
	L_D, nm	10	5	3	2

The main photovoltaic properties of SC OSCs are presented in Fig. 6 and summarized in Table 3 (averaged photovoltaic parameters are presented in ESI, Table S5.1). Thermal and solvent vapor annealing methods for optimizing the active layer morphology were applied for the solar cells fabricated from **1T**, **3T,** and **4T** molecules as they are able to form ordered structures as per the X-ray data (ESI, Fig.S3.2b). However, both methods did not result in an increased PCE. Possibly, the low thickness of the films, which is optimal for the OSC operation, complicates their ordering observed in the thicker films [45].

As expected, the **0T**-based SC OSCs did not work, which we assign to the absence of observable electron transport. Other SC OSCs differ mainly in J_{SC} and V_{OC}, whereas the FF values are almost the same (~25%). The low fill factor (FF) could be explained by a strong dependence of the charge photogeneration efficiency on the electric field because the current density does not saturate at the negative voltages (Fig. 6a). The **1T**, **2T**, **3T,** and **4T**-based SC OSCs showed very high V_{OC} values, which are among the highest ones for SC OSCs [6]. The **1T**-based SC OSCs showed lower V_{OC}, which does not correspond to the largest band gap (Fig. 4c). This lower V_{OC} can be associated with the increased charge recombination losses owing to the less efficient charge transport. The J_{SC} values increase monotonically with increasing the oligothiophene π-bridge length from 1 to 4. The J_{SC} values calculated from the external quantum effeciency (EQE) spectra are in good agreement with the J_{SC} value obtained from the *J-V* curves (Table 3). In general, the EQE spectra follow the absorption spectra. The **3T** and **4T**-based devices showed the most red-shifted EQE spectra, and the latter had the highest EQE values resulting in the highest J_{SC}. In contrast, **1T**-based devices demonstrated the most blue-shifted EQE spectrum and lowest EQE values and hence the lowest J_{SC} value. Thus, the trend of increasing the efficiency of SC OSCs based on the considered series of molecules with increasing the π-bridge length was revealed, which is in accordance with the conclusions of work [20]. In fact, as per the field-assisted charge generation mechanism [58], the farther the donor and acceptor units are spatially separated, the easier the excitons are separated under the applied electric field.

Table 3
The best photovoltaic parameters of SC OSCs under AM1.5G illumination (100 mW/cm^2), maximum EQEs, responsivities (R), and rise times of the photodetectors.

Active layer material	J_{SC}, mA/cm^2	$J_{SC\ EQE}$[a], mA/cm^2	V_{OC}, V	FF, %	PCE, %	EQE, %	R, A/W	Rise time, μs
0T	-[b]	–	–	–	–	–	–	–
1T	0.25	0.20	1.08	22.1	0.06	1.9	0.008	-[c]
2T	1.70	1.55	1.13	24.3	0.47	11.8	0.052	0.74 ± 0.05
3T	3.21	2.85	1.14	26.0	0.95	19.5	0.088	0.85 ± 0.06
4T	3.64	3.16	1.03	29.0	1.09	22.6	0.097	1.09 ± 0.10

Note: [a] $J_{SC\ EQE}$ is the short-circuit current integrated from the EQE spectrum. [b] These devices did not show any photocurrent. [c] Owing to a weak signal, the rise rime was not measured.

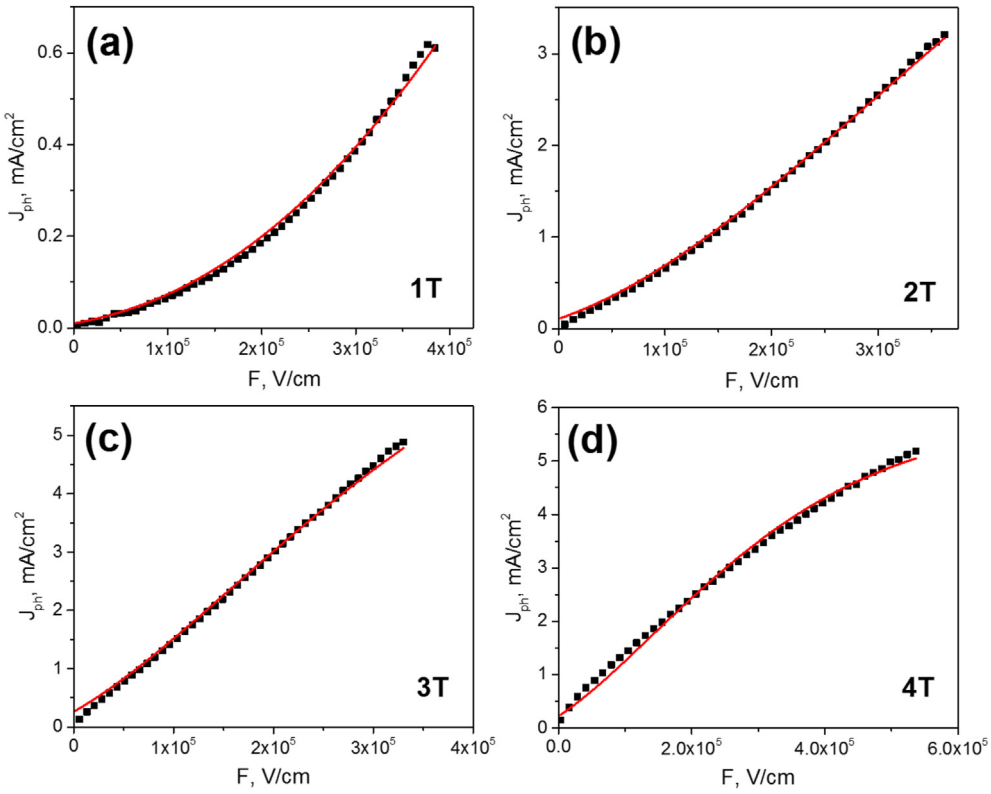

Fig. 7. Dependences of the photocurrent on the electric field (black squares) and Onsager model fit (red lines) (Eq. [S5.3]) for **1T** (**a**), **2T** (**b**), **3T** (**c**), and **4T** (**d**). Note a non-zero charge yield at zero electric field in full accordance with the Onsager model. (For interpretation of the references to color in this figure legend, the reader is referred to the Web version of this article.)

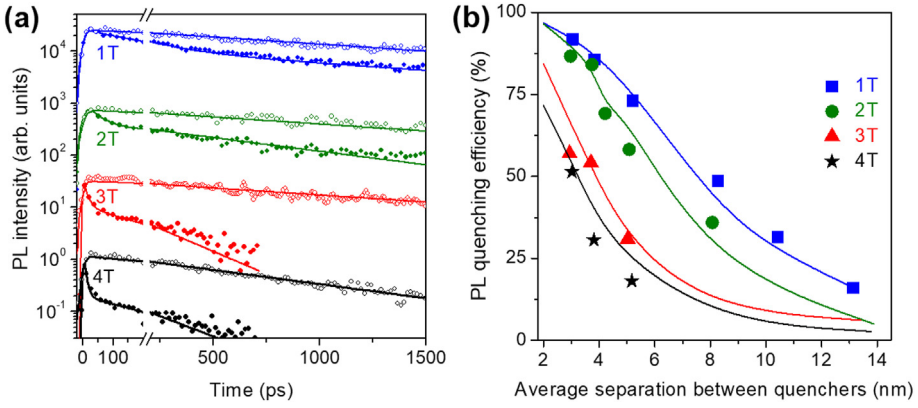

Fig. 8. PL transients (**a**) and PL-quenching efficiencies (**b**) for **1T-4T** compounds. (**a**) Experimental PL transient data in the matrices and neat films are depicted by open and close circles, respectively, whereas the solid lines show the respective fitting convoluted with a Gaussian apparatus function of ~ 3–10 ps. The blue color corresponds to **1T**, green is **2T**, red is **3T,** and black is **4T**. For clarity, the PL transients of **1T**, **2T,** and **3T** are offset by multiplying by a factor of 30 with respect to the previous transient. (**b**) PL-quenching efficiency versus average separation between quenchers for **1T** (blue square), **2T** (green circle), **3T** (red triangle), and **4T** (black star). The PL-quenching efficiency and average separation between quenchers were determined as described in ESI, Section 6.4. The solid lines are the Monte-Carlo modeled results (ESI, Section 6.5). (For interpretation of the references to color in this figure legend, the reader is referred to the Web version of this article.)

Because the photocurrent generation in the SC OSC studied is more efficient at negative bias, they could be used as photodetectors. Fig. 6d presents responsivity spectra of the photodetectors. The responsivity quantifies the ability of a photodetector to convert optical power to the electric current. The responsivity values of SC **2T**-**4T**-based photodetectors are comparable to those having more complicated structures, for example, BHJ organic and perovskite/organic hybrid photodetectors [59,60]. Moreover, the responsivity of our SC photodetectors in the blue spectral range is comparable with commercial silicon photodetectors.

We also studied time-resolved response of the photodetectors to a rectangular optical pulse (the measurement details are described in Section 1.5 of ESI). The rise times of the photodetector response are summarized in Table 3 (the transients presented in ESI, Section 5.7): they are about 1 μs or shorter and systematically increase with **nT** (n = 2–4). Among a plethora of factors affecting the rise time, the main ones are the charge mobility values, exciton dynamics, charge generation rate, applied voltage, and *RC* time constant [60]. The exciton lifetime drops with the increase of **nT** (Table 4) well below 1 ns; therefore, the delayed charge generation

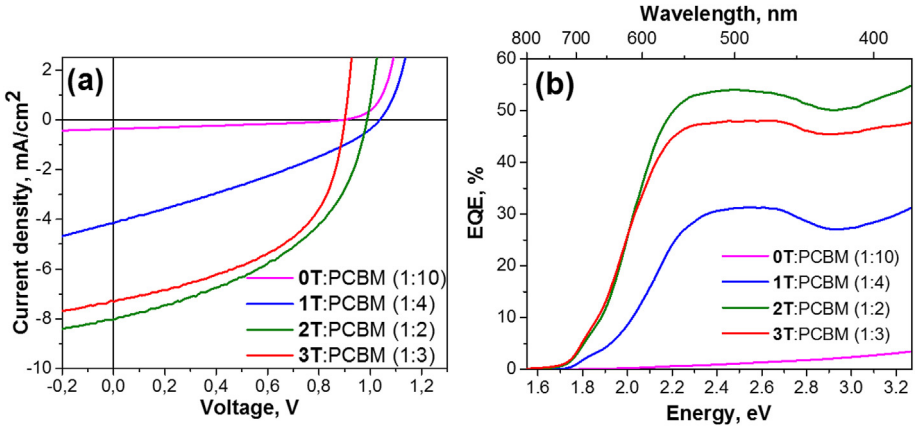

Fig. 9. *J-V* curves under AM1.5G illumination (100 mW/cm^2) (**a**) and EQE spectra (**b**) for BHJ solar cells.

Table 5
The best photovoltaic parameters of BHJ solar cells under AM1.5G illumination (100 mW/cm^2), maximum EQE values, hole mobilities in blends.

Active layer material	J_{SC}, mA/cm^2	$J_{SC\ EQE}$[a], mA/cm^2	V_{OC}, V	FF, %	PCE, %	EQE, %	$\mu_h \cdot 10^{-4}$, cm^2/(Vs)
0T:PC$_{71}$BM (1:10)	0.37	0.18	0.89	31.1	0.10	3.5	4.3 ± 0.4
1T:PC$_{71}$BM (1:4)	4.14	3.87	1.04	31.8	1.37	31.3	4.9 ± 1.7
2T:PC$_{71}$BM (1:2)	8.03	7.68	0.99	45.1	3.59	54.7	9.8 ± 1.1
3T:PC$_{71}$BM (1:3)	7.30	7.06	0.90	50.5	3.31	48.0	9.7 ± 2.7

Note: [a] $J_{SC\ EQE}$ is the short-circuit current integrated from the EQE spectrum.

at a submicrosecond time scale hardly can be a reason for the increase in the photodetector rise time with **nT**. We assign the increase in the rise time to variation of the hole mobility value with **nT**. Indeed, more excitons and hence electron-hole pairs are generated near the transparent electrode, which collects the electrons in the inverted device architecture used (for details see ESI, Section 1.5.1). Therefore, the hole mobility value plays a key role in the photodetector transient response as the holes must pass through the thickness of the active layer. The time (t) of flight of a hole through the thickness (d) of the active layer is estimated as $t = d/\mu_{h\times}F$, where F is the internal electric field (see 2.4.2). As a result, the time of flight increases from 0.15 to 0.4 μs with **nT**. Accordingly, the hole mobility decreases with increasing of the π-bridge length (Table 2) is the most likely reason for the longer rise times of the corresponding photodetectors (Table 3).

Although the measured photodetector rise times are not record-breaking, they along with the high responsivity values are sufficient for the use, for example, as photosensitive materials the in artificial human retina with tunable position of the absorption maximum to mimic human eye cones and rods as recently was demonstrated for similar small D-A molecules [61].

2.4.2. Charge generation yield

For SC OSCs based on **1T**–**4T,** the current density does not saturate at the negative voltages indicating a strong dependence of the charge photogeneration efficiency on the electric field. Fig. 7 demonstrates the photocurrent obtained from *J-V* characteristics (Fig. 6a) and replotted as a function of the internal electric field (F). The photocurrent was calculated as the difference between the current density under light and in the dark. The internal field was calculated as $F=(V_{BI}-V)/d$, where d is the active layer thickness, V_{BI} is the built-in voltage that was taken as a voltage at which the photocurrent is equal to zero.

As was demonstrated earlier, the field dependence of the photocurrent of SC OSCs based on N(Ph-2T-DCV-Et)$_3$ (it differs from **2T** only by alkyl terminal groups) was well-described by the linearized Onsager model [20], which explained the strong field dependence of charge photogeneration. However, the effect of the π-bridge length between donor and acceptor units on the charge pair separation was not studied. After the Onsager model, from fitting the experimental data in Fig. 7, we calculated the initial intrapair separation of photogenerated charges, r_0 (the calculation details are presented in the ESI, see Section 5.5). Note that charge dissociation occurs both from intramolecular and intermolecular CT excitons (see the next section). As a result, we found that an increase in the number of thiophenes between the donor and acceptor blocks in a series **1T** → **2T** → **3T** → **4T** results in an increase in r_0: 2.9 nm → 4.4 nm → 5.5 nm → 5.8 nm. Therefore, r_0 is well-correlated with the length of the thiophene bridge. This is quite reasonable as a longer bridge results in less CT exciton binding energy facilitating generation of separated charges. The charge pair dissociation efficiency depends on the ratio of r_0 to the Coulombic capture radius $r_c = q^2/4\pi\varepsilon_0\varepsilon kT$ = 19 nm, where q is the elementary charge, ε_0 is the dielectric constant, ε = 3 is the dielectric permittivity, k is the Boltzmann constant, and T = 295 K is the temperature. As r_0 is 3–6 times shorter than r_c, one needs additional energy to split the CT exciton into a pair of free charges. This energy can be gained from the applied electric field, and this explains the strong field dependence of charge photogeneration. Note that the fit of the experimental data in Fig. 7 was also performed as per the Onsager-Braun model (for details see the ESI, Section 5.5)), which is well-accepted for D-A systems. But this model greatly underestimated the photocurrent in **1T**–**4T** at low electric fields. The most probable reason for this is that, in contrast to D-A heterojunction devices, where the lowest CT state — an intermediate in the exciton-to-free-charge pathway — lies much below the exciton state, in our SC OSCs, the intramolecular and intermolecular excitons are CT ones, and they are expected to be close in energy. This is supported by the X-ray data (Fig. S3.2): the distances between donor and acceptor units of one molecule and between donor and acceptor units of neighboring molecules are close. Thus, we conclude that the Onsager model adequately describes the photogeneration of free charges in our SC OSCs.

2.4.3. Time-resolved PL

More insights into the processes of charge generation and the correlations demonstrated in the previous section were obtained by time-resolved PL studies of the **1T**–**4T** films. Fig. 8a shows PL transients in matrices and neat films obtained by integrating the PL maps (ESI, Section 6.1) in the 550–820 nm (2.25–1.50 eV) spectral range. The molecules dispersed in the poly(methyl methacrylate) (PMMA) matrix at low concentration were used as a reference solid-state environment without intermolecular interactions (ESI, Section 6.2) [62–66]. All the matrices exhibit monoexponential decays with a lifetime of 1600 ps for **1T**, **2T**, **3T**, and 800 ps for **4T** (see Table 4 for fitting parameters). The shorter lifetime of the **4T** matrix as compared with other molecules could be owing to more efficient intramolecular CT excitation recombination caused by torsions of the long thiophene bridge [66].

In sharp contrast to the matrix measurements, all the molecules demonstrate biexponential PL transients in the neat films. There is a clear decrease in exciton lifetime with the elongation of the oligothiophene bridge (**nT, n=1–4**). The shortest component decreases from 200 ps to 10 ps from **1T** to **4T**, and its share increases (Table 4). By using time-resolved photoinduced absorption and time-resolved PL spectroscopies, Kozlov et al. [63,66] demonstrated that in neat films of densely packed star-shaped small molecules efficient exciton-to-polaron conversion occurs within the first 100 ps, which leads to generation of intermolecular CT excitons. Similarly, we assign the shortest (within the first 100 ps) components of PL transient decay in the **nT** star-shaped molecules to the formation of intermolecular CT excitons, which facilitates the generation of quasi-free charges [63–66]. This is in line with the increasing values of the maximum EQE spectra (Fig. 6b), the respective J_{sc} values (Table 3), and an increase in the radius of the initial charge separation (Section 2.4.2) observed from **1T** to **4T**.

The slower component in the PL transients is attributed to delayed formation of the intermolecular CT excitons during exciton diffusion. The share of this component gradually decreases from ~0.4 in **1T** to ~0.1 in **4T** (Table 4) making the almost immediate formation of the intermolecular CT excitons the dominant channel. This corroborates the conclusion from the previous section that when the energies of intramolecular and intermolecular CT states are close as well as the intramolecular and intermolecular distances between the donor and acceptor units (Fig. S3.2) the formation of intermolecular excitons dominates for the following reason. Each donor unit is surrounded by more than three acceptor units belonging to other molecules, making intermolecular charge separation (the hole at the original donor unit and the electron at an acceptor unit of a different molecule) more probable. Note that both increase in the lifetimes and disappearance of the fast-decaying PL component in the matrix signify no formation of the intermolecular CT excitons owing to the lack of intermolecular interactions.

The lifetimes were derived from exponential (biexponential for films) fits of the PL transients. The values in parenthesis show shares of the exponents. The average exciton lifetime was determined as $\tau_{avg} = \frac{\sum_i a_i \tau_i^2}{\sum_i a_i \tau_i}$. Note that 10 ps delay is at the verge of the apparatus resolution. We define the efficiency Q_{CTE} of formation of the intermolecular CT excitons as $Q_{CTE} = 1 - \frac{\tau_{avg}}{\tau}$, where τ_{avg} is the average PL lifetime in the neat films, and τ is the PL lifetime in the PMMA matrix. Hence, in the neat films $Q_{CTE} = 13\%$, 50%, 85%, and 75% for **1T**, **2T**, **3T,** and **4T**, respectively. This implies that for **3T** and **4T** there are only 15% and 25% excitons available for subsequent diffusion, whereas for **1T** and **2T,** this number increases to 87% and 50%, respectively. The obtained results demonstrate the efficiency of exciton dissociation in the solution-processed neat films of the star-shaped molecules, especially for **3T** and **4T**, rendering them highly suitable for SC OSCs.

2.4.4. Exciton diffusion

The next issue to address is the distance over which the excitons can diffuse. The knowledge of exciton diffusion length (L_D) is an essential aspect to be considered for morphology optimization of BHJ solar cells [67–72] but least important for SC OSCs if fast formation of the charge-separated state is facilitated. To investigate the exciton diffusion in solution-processed BHJ films, time-resolved volume-quenching experiments (ESI, Section 6.4) were performed [73]. The fullerene derivative $PC_{60}BM$ was used as a quencher molecule and dispersed at different concentrations in the films of the molecules under investigation. Fig. 8b summarizes the PL-quenching efficiency as a function of average separation between the quenchers (see ESI, Section 6.4 for calculations details). For all the molecules, the PL-quenching efficiency is minimal at large separation between quenchers (i.e. at low $PC_{60}BM$ concentrations). Considerable quenching is achieved when the average separation between quenchers is short.

To obtain quantitative information about the effect of the oligothiophene bridge length (**nT,** n = 1–4) on exciton dynamics, we performed Monte-Carlo simulations to extract the values of exciton diffusion lengths (for more details, see ESI, Section 6.5). The exciton diffusion lengths amount to ~10 nm, ~5 nm, ~3 nm, and ~2 nm for **1T**, **2T, 3T,** and **4T** (Table 4), respectively, which are mostly determined by the short exciton lifetimes. Note that owing to fast initial decay of PL transients in **3T** and **4T** (Fig. 8a) approaching or even exceeding the apparatus resolution, the uncertainty in exciton displacement might be quite substantial. The short exciton diffusion length is not detrimental for high-performance SC OSCs as charge photogeneration occurs in the bulk. This is in contrast with heterojunction OSCs, where the exciton has to diffuse to the interface of the donor and acceptor phases for its dissociation (see the next section).

The obtained results demonstrate a clear correlation of the exciton diffusion length with the length of the oligothiophene bridge, **nT**. Similarly, to the exciton lifetime, the exciton diffusion length decreases with increase of **nT**. Therefore, we presume that these two are interconnected, that is, the intramolecular CT state is transferred to the intermolecular CT exciton almost immediately (within the experimental time resolution of ~10 ps) if the energetic conditions are favorable, otherwise the formation of intermolecular CT exciton is delayed, so that the intramolecular exciton can contribute to the exciton diffusion process (ESI, Section 6.5). The exciton diffusion lengths are anticorrelated with the initial charge separation distances (Section 2.4.2), which can be explained as follows: when the charges are considerable apart (i.e. in the intermolecular state), they mostly undergo nonradiative recombination.

2.4.5. BHJ solar cells

Fig. 9 compares *J-V* curves and EQE spectra of $PC_{71}BM$-based solar cells, and their photovoltaic properties are summarized in Table 5 (averaged photovoltaic parameters are presented in ESI, Table S5.2). Owing to the poor solubility of the **4T,** we were not able to fabricate working devices based on **4T**:$PC_{71}BM$. We compared BHJ solar cells with the optimal D-A mass ratios because the **0T**–**3T** has significantly different molecular weights (the optimization data are presented in ESI, Section 5.6). We did not apply annealing to BHJ devices as it was useless for SC and similar BHJ OSCs as reported in our previous works [44,45].

PCEs of BHJ solar cells followed a different trend in contrast to the SC OSCs, the π-bridge length of two thiophenes was optimal for the highest performance of BHJ solar cells based on blends with $PC_{71}BM$. Solar cells based on **2T** had the highest J_{SC} in accordance with the highest EQE. The various V_{OC} values correspond to the different HOMO energies of molecules with the

different π-bridge lengths (Fig. 4c). The low V_{OC} value for the **0T**:$PC_{71}BM$ blend could be assigned to the too low donor mass fraction in the blend.

The different performance of the **0T**–**3T** BHJ solar cells (namely, the different J_{SC}, EQE, and FF values) could be explained by the corresponding differences in the exciton diffusion lengths and charge mobilities as detailed below. Indeed, the better performance of the **2T-**based BHJ solar cells as compared with that of **3T-**based ones may be explained by the longer exciton diffusion length in the former as shown in the previous section. Note that the AFM data (Fig. S5.15) for **0T**–**3T**-blended films demonstrated smooth surfaces with indistinguishable morphologies, and this is a sign of inessential differences in the bulk morphology. The measured hole mobilities in the blended films (Fig. S5.10 – S5.13, Table 5) shows that the **2T** and **3T-**based blends had the highest hole mobilities in agreement with the hole transport data in the pristine films (Table 2) and the highest J_{SC} and FF values of the respective BHJ solar cells. Noteworthy, the blended films demonstrated higher hole mobilities than those in the pristine films. Similar enhancement of the hole transport in blends was observed earlier in the polymer-fullerene blends, which was tentatively assigned to more favorable polymer packing in the donor phase [74]. Note that, in all the blends studied, the electron mobilities are assumed to be similar as they are determined mainly by $PC_{71}BM$.

3. Conclusions

In summary, the series of triphenylamine-based star-shaped D-π-A small molecules differing by the number of thiophenes in the arms from 0 to 4 were synthesized and comprehensively studied. The variation of the oligothiophene π-bridge length from 0 to 4 units leads to a significant decrease in solubility from 220 to 1 gL^{-1} and increase in glass transition temperature from 14 to 94 °C. The elongation of the π-bridge leads also to a bathochromic shift of the absorption spectra, increasing of the HOMO energies, and narrowing of the bandgap. **1T**–**4T** films show relatively balanced ambipolar charge transport and work in SC OSCs with high V_{OC} (up to 1.14 eV). The J_{SC} values and PCE increase with elongation of the π-bridge from 0.06% (**1T**) to the remarkable 1.1% (**4T**), which is among the highest values for the SC OSCs based on simple D-A molecules. These conclusions are supported by the Onsager theory calculations as well as the time-resolved PL spectroscopy experiments, which revealed that the more spatially separated the donor and acceptor units, that is, the longer the π-bridge, the more efficiently the dissociation of intramolecular and intermolecular excitons occurs, and hence more free charges are generated. In general, the trend of the PCE increases with the π-bridge length preserves also for BHJ OSCs with $PC_{71}BM$ as the acceptor. Besides SC OSCs and BHJ OSCs, such molecules can operate in a single-component organic photodetector. From the results obtained, we conclude that the length of the conjugated π-bridge in D-A star-shaped small molecules strongly impacts the physicochemical, photophysical, and charge transport properties of the films and the performance of photovoltaic devices. We expect that the conclusions outlined therein will contribute to the further development of D-A small molecules for highly efficient organic photovoltaic devices.

Data availability statement

The raw/processed data required to reproduce these findings cannot be shared at this time owing to technical or time limitations.

Author contributions

Yuriy N. Luponosov: Conceptualization; Writing – original draft, Recourses, Writing – review & editing, Supervision; Alexander N. Solodukhin: Resourses; Writing – original draft; Artur L. Mannanov: Investigation; Writing – review & editing; Petr S. Savchenko: Investigation; Benedito A. L. Raul: Investigation; Writing – review & editing; Svetlana M. Peregudova: Investigation; Nikolay M. Surin: Investigation; Artem V. Bakirov: Investigation; Writing – review & editing; Maxim A. Shcherbina: Formal analysis; Writing – review & editing; Sergei N. Chvalun: Methodology; Supervision; Maxim S. Pshenichnikov: Methodology; Writing – review & editing; Supervision; Dmitry Yu. Paraschuk: Conceptualization; Writing – review & editing; Supervision; Sergey A. Ponomarenko: Writing – review & editing; Project administration.

Declaration of competing interest

The authors declare that they have no known competing financial interests or personal relationships that could have appeared to influence the work reported in this article.

Acknowledgments

The work was supported by the Russian Science Foundation (grant number 19-73-30028). B.A.L.R. and M.S.P. acknowledge funding from the European Union's Horizon 2020 research and innovation program under the Marie Skłodowska-Curie grant agreement № 722651 (SEPOMO). NMR and UV–vis absorption and luminescence spectra were recorded using the equipment of Collaborative Access Center 'Center for Polymer Research' of the Enikolopov Institute of Synthetic Polymeric Materials of the Russian Academy of Sciences with the financial support from the Ministry of Science and Higher Education of the Russian Federation (Contract 0071-2021-0005). The work on solar cells was performed using the equipment purchased under the Lomonosov Moscow State University Program of Development. B.A.L.R. and M.S.P. thank F. de Haan for general laboratory assistance and Sylvia Rousseva for preparing the neat and mixed films for time-resolved photoluminescence measurements.

Appendix A. Supplementary data

Supplementary data to this article can be found online at https://doi.org/10.1016/j.mtener.2021.100863.

References

[1] M.A. Green, Y. Hishikawa, E.D. Dunlop, D.H. Levi, J. Hohl-Ebinger, A.W.Y. Ho-Baillie, Solar cell efficiency tables (version 52), Prog. Photovoltaics Res. Appl. 26 (2018) 427–436, https://doi.org/10.1002/pip.3040.
[2] L. Meng, Y. Zhang, X. Wan, C. Li, X. Zhang, Y. Wang, X. Ke, Z. Xiao, L. Ding, R. Xia, H.-L. Yip, Y. Cao, Y. Chen, Organic and solution-processed tandem solar cells with 17.3% efficiency, Science 361 (2018) 1094–1098, https://doi.org/10.1126/science.aat2612.
[3] Q. Liu, Y. Jiang, K. Jin, J. Qin, J. Xu, W. Li, J. Xiong, J. Liu, Z. Xiao, K. Sun, S. Yang, X. Zhang, L. Ding, 18% Efficiency organic solar cells, Sci. Bull. 65 (2020) 272–275, https://doi.org/10.1016/j.scib.2020.01.001.
[4] A. Cravino, P. Leriche, O. Alévêque, S. Roquet, J. Roncali, Light-emitting organic solar cells based on a 3D conjugated system with internal charge transfer, Adv. Mater. 18 (2006) 3033–3037, https://doi.org/10.1002/adma.200601230.
[5] J. Roncali, Single material solar cells: the next frontier for organic photovoltaics? Adv. Energy Mater. 1 (2011) 147–160, https://doi.org/10.1002/aenm.201000008.
[6] J. Roncali, I. Grosu, The dawn of single material organic solar cells, Adv. Sci. 6 (2019) 1801026, https://doi.org/10.1002/advs.201801026.
[7] P. Yu, G. Feng, J. Li, C. Li, Y. Xu, C. Xiao, W. Li, A selenophene substituted double-cable conjugated polymer enables efficient single-component organic solar cells, J. Mater. Chem. C. 8 (2020) 2790–2797, https://doi.org/10.1039/C9TC06667E.

[8] Y. Zhang, D. Deng, Q. Wu, Y. Mi, C. Yang, X. Zhang, Y. Yang, W. Zou, J. Zhang, L. Zhu, H. Zhou, X. Liu, Z. Wei, High-efficient charge generation in single-donor-component-based p-i-n structure organic solar cells, Sol. RRL. 4 (2020) 1900580, https://doi.org/10.1002/solr.201900580.
[9] L. Zhu, J. Zhang, Y. Guo, C. Yang, Y. Yi, Z. Wei, Small exciton binding energies enabling direct charge photogeneration towards low-driving-force organic solar cells, Angew. Chem. Int. Ed. 60 (2021) 15348–15353, https://doi.org/10.1002/anie.202105156.
[10] X. Jiang, J. Yang, S. Karuthedath, J. Li, W. Lai, C. Li, C. Xiao, L. Ye, Z. Ma, Z. Tang, F. Laquai, W. Li, Miscibility-controlled phase separation in double-cable conjugated polymers for single-component organic solar cells with efficiencies over 8 %, Angew. Chem. 132 (2020) 21867–21876, https://doi.org/10.1002/ange.202009272.
[11] Y. Dong, V.C. Nikolis, F. Talnack, Y.-C. Chin, J. Benduhn, G. Londi, J. Kublitski, X. Zheng, S.C.B. Mannsfeld, D. Spoltore, L. Muccioli, J. Li, X. Blase, D. Beljonne, J.-S. Kim, A.A. Bakulin, G. D'Avino, J.R. Durrant, K. Vandewal, Orientation dependent molecular electrostatics drives efficient charge generation in homojunction organic solar cells, Nat. Commun. 11 (2020) 4617, https://doi.org/10.1038/s41467-020-18439-z.
[12] H. Bin, J. Yao, Y. Yang, I. Angunawela, C. Sun, L. Gao, L. Ye, B. Qiu, L. Xue, C. Zhu, C. Yang, Z.-G. Zhang, H. Ade, Y. Li, High-efficiency all-small-molecule organic solar cells based on an organic molecule donor with alkylsilyl-thienyl conjugated side chains, Adv. Mater. 30 (2018) 1706361, https://doi.org/10.1002/adma.201706361.
[13] J. Roncali, P. Leriche, P. Blanchard, Molecular materials for organic photovoltaics: small is beautiful, Adv. Mater. 26 (2014) 3821–3838, https://doi.org/10.1002/adma.201305999.
[14] S.D. Collins, N.A. Ran, M.C. Heiber, T.-Q. Nguyen, Small is powerful: recent progress in solution-processed small molecule solar cells, Adv. Energy Mater. 7 (2017) 1602242, https://doi.org/10.1002/aenm.201602242.
[15] A. Bogdan, L. Szolga, G.-I. Giurgi, A.P. Crişan, D. Bogdan, S. Hadsadee, S. Jungsuttiwong, R. Po, I. Grosu, J. Roncali, Structure-properties relationships in triarylamine-based push-pull systems-C60 dyads as active material for single-material organic solar cells, Dye. Pigment. 184 (2021) 108845, https://doi.org/10.1016/j.dyepig.2020.108845.
[16] S. Lucas, J. Kammerer, M. Pfannmöller, R.R. Schröder, Y. He, N. Li, C.J. Brabec, T. Leydecker, P. Samorì, T. Marszalek, W. Pisula, E. Mena-Osteritz, P. Bäuerle, Molecular donor–acceptor dyads for efficient single-material organic solar cells, Sol. RRL. 5 (2021) 2000653, https://doi.org/10.1002/solr.202000653.
[17] Y. Li, J.-Y. Liu, Y.-D. Zhao, Y.-C. Cao, Recent advancements of high efficient donor–acceptor type blue small molecule applied for OLEDs, Mater. Today 20 (2017) 258–266, https://doi.org/10.1016/j.mattod.2016.12.003.
[18] A.L. Kanibolotsky, I.F. Perepichka, P.J. Skabara, Star-shaped π-conjugated oligomers and their applications in organic electronics and photonics, Chem. Soc. Rev. 39 (2010) 2695, https://doi.org/10.1039/b918154g.
[19] O.V. Kozlov, Y.N. Luponosov, S.A. Ponomarenko, N. Kausch-Busies, D.Y. Paraschuk, Y. Olivier, D. Beljonne, J. Cornil, M.S. Pshenichnikov, Ultrafast charge generation pathways in photovoltaic blends based on novel star-shaped conjugated molecules, Adv. Energy Mater. 5 (2015) 1401657, https://doi.org/10.1002/aenm.201401657.
[20] A.L. Mannanov, P.S. Savchenko, Y.N. Luponosov, A.N. Solodukhin, S.A. Ponomarenko, D.Y. Paraschuk, Charge photogeneration and recombination in single-material organic solar cells and photodetectors based on conjugated star-shaped donor-acceptor oligomers, Org. Electron. 78 (2020) 105588, https://doi.org/10.1016/j.orgel.2019.105588.
[21] L.-N. Wu, M.-Y. Li, M.-Y. Sui, J.-C. Huang, G.-Y. Sun, L. Cheng, Achieve panchromatic absorption for all-small-molecule organic solar cells based on mono-porphyrin molecules by π-bridge modification, Materials Today Energy 20 (2021) 100658, https://doi.org/10.1016/j.mtener.2021.100658.
[22] T. Otsubo, Y. Aso, K. Takimiya, Functional oligothiophenes as advanced molecular electronic materials, J. Mater. Chem. 12 (2002) 2565–2575, https://doi.org/10.1039/b203780g.
[23] A. Mishra, C.-Q. Ma, P. Bäuerle, Functional oligothiophenes: molecular design for multidimensional nanoarchitectures and their applications, Chem. Rev. 109 (2009) 1141–1276, https://doi.org/10.1021/cr8004229.
[24] K. Schulze, C. Uhrich, R. Schüppel, K. Leo, M. Pfeiffer, E. Brier, E. Reinold, P. Bäuerle, Efficient vacuum-deposited organic solar cells based on a new low-bandgap oligothiophene and fullerene C60, Adv. Mater. 18 (2006) 2872–2875, https://doi.org/10.1002/adma.200600658.
[25] Y. Liu, X. Wan, F. Wang, J. Zhou, G. Long, J. Tian, J. You, Y. Yang, Y. Chen, Spin-coated small molecules for high performance solar cells, Adv. Energy Mater. 1 (2011) 771–775, https://doi.org/10.1002/aenm.201100230.
[26] B. Walker, C. Kim, T.-Q. Nguyen, Small molecule solution-processed bulk heterojunction solar cells, Chem. Mater. 23 (2011) 470–482, https://doi.org/10.1021/cm102189g.
[27] A. Mishra, P. Bäuerle, Small molecule organic semiconductors on the move: promises for future solar energy technology, Angew. Chem. Int. Ed. 51 (2012) 2020–2067, https://doi.org/10.1002/anie.201102326.
[28] H. Muraoka, S. Ogawa, Synthesis and electrochemical properties of ferrocene dimers and trimers bridged by an oligothiophene spacer, Pure Appl. Chem. 85 (2012) 777–784, https://doi.org/10.1351/PAC-CON-12-06-14.
[29] K. Arja, M. Elgland, K.P.R. Nilsson, Synthesis and characterization of oligothiophene–porphyrin-based molecules that can Be utilized for optical assignment of aggregated amyloid-β morphotypes, Front. Chem. 6 (2018) 391, https://doi.org/10.3389/fchem.2018.00391.
[30] X. Wan, C. Li, M. Zhang, Y. Chen, Acceptor–donor–acceptor type molecules for high performance organic photovoltaics – chemistry and mechanism, Chem. Soc. Rev. 49 (2020) 2828–2842, https://doi.org/10.1039/D0CS00084A.
[31] F. Würthner, F. Effenberger, R. Wortmann, P. Krämer, Second-order polarizability of donor—acceptor substituted oligothiophenes: substituent variation and conjugation length dependence, Chem. Phys. 173 (1993) 305–314, https://doi.org/10.1016/0301-0104(93)80147-2.
[32] G.R. Kumar, S.K. Sarkar, P. Thilagar, Aggregation-induced emission and sensing characteristics of triarylborane-oligothiophene-dicyanovinyl triads, Chem. Eur J. 22 (2016) 17215–17225, https://doi.org/10.1002/chem.201603349.
[33] N.K. Kalinichenko, D.O. Balakirev, P.S. Savchenko, A.L. Mannanov, S.M. Peregudova, D Yu Paraschuk, S.A. Ponomarenko, Yu N. Luponosov, Effects of electron-withdrawing group and π-conjugation length in donor-acceptor oligothiophenes on their properties and performance in non-fullerene organic solar cell, Dyes Pigments 194 (2021) 109592, https://doi.org/10.1016/j.dyepig.2021.109592.
[34] D.A. Doval, M.D. Molin, S. Ward, A. Fin, N. Sakai, S. Matile, Planarizable push–pull oligothiophenes: in search of the perfect twist, Chem. Sci. 5 (2014) 2819–2825, https://doi.org/10.1039/C4SC00939H.
[35] V. Hernández, J. Casado, F. Effenberger, J.T. López Navarrete, Analysis of the intramolecular charge transfer in donor–acceptor α,α′-substituted oligothiophenes from their vibrational spectra, J. Chem. Phys. 112 (2000) 5105–5112, https://doi.org/10.1063/1.481066.
[36] J. Roncali, P. Leriche, A. Cravino, From one- to three-dimensional organic semiconductors: in search of the organic silicon? Adv. Mater. 19 (2007) 2045–2060, https://doi.org/10.1002/adma.200700135.
[37] A.N. Solodukhin, Y.N. Luponosov, A.L. Mannanov, P.V. Dmitryakov, S.M. Peregudova, S.N. Chvalun, D.Y. Parashchuk, S.A. Ponomarenko, Effect of branching on the physical and photovoltaic properties of donor–acceptor oligomers based on triphenylamine, Mendeleev Commun. 29 (2019) 385–387, https://doi.org/10.1016/j.mencom.2019.07.008.
[38] M.-Y. Li, H. Yin, G.-Y. Sun, PDI derivatives with functional active position as non-fullerene small molecule acceptors in organic solar cells: from different core linker to various conformation, Applied Materials Today 21 (2020) 100799, https://doi.org/10.1016/j.apmt.2020.100799.
[39] A.N. Solodukhin, Y.N. Luponosov, A.L. Mannanov, P.S. Savchenko, A.V. Bakirov, M.A. Shcherbina, S.N. Chvalun, D.Y. Paraschuk, S.A. Ponomarenko, Branched electron-donor core effect in D-π-A star-shaped small molecules on their properties and performance in single-component and bulk-heterojunction organic solar cells, Energies 14 (2021) 3596, https://doi.org/10.3390/en14123596.
[40] J. Wang, K. Liu, L. Ma, X. Zhan, Triarylamine: versatile platform for organic, dye-Sensitized, and perovskite solar cells, Chem. Rev. 116 (23) (2016) 14675–14725, https://doi.org/10.1021/acs.chemrev.6b00432.
[41] S. Roquet, A. Cravino, P. Leriche, O. Alévêque, P. Frère, J. Roncali, Triphenylamine–Thienylenevinylene hybrid systems with internal charge transfer as donor materials for heterojunction solar cells, J. Am. Chem. Soc. 128 (2006) 3459–3466, https://doi.org/10.1021/ja058178e.
[42] E. Ripaud, Y. Olivier, P. Leriche, J. Cornil, J. Roncali, Polarizability and internal charge transfer in thiophene–triphenylamine hybrid π-conjugated systems, J. Phys. Chem. B 115 (2011) 9379–9386, https://doi.org/10.1021/jp203759e.
[43] J. Cremer, P. Bäuerle, Star-shaped perylene–oligothiophene–triphenylamine hybrid systems for photovoltaic applications, J. Mater. Chem. 16 (2006) 874–884, https://doi.org/10.1039/B515657B.
[44] J. Min, Y.N. Luponosov, D. Baran, S.N. Chvalun, M.A. Shcherbina, A.V. Bakirov, P.V. Dmitryakov, S.M. Peregudova, N. Kausch-Busies, S.A. Ponomarenko, T. Ameri, C.J. Brabec, Effects of oligothiophene π-bridge length on physical and photovoltaic properties of star-shaped molecules for bulk heterojunction solar cells, J. Mater. Chem. A. 2 (2014) 16135–16147, https://doi.org/10.1039/C4TA01933D.
[45] J. Min, Y.N. Luponosov, A. Gerl, M.S. Polinskaya, S.M. Peregudova, P.V. Dmitryakov, A.V. Bakirov, M.A. Shcherbina, S.N. Chvalun, S. Grigorian, N. Kaush-Busies, S.A. Ponomarenko, T. Ameri, C.J. Brabec, Alkyl chain engineering of solution-processable star-shaped molecules for high-performance organic solar cells, Adv. Energy Mater. 4 (2014) 1301234, https://doi.org/10.1002/aenm.201301234.
[46] M.J. Parker, Test methods for physical properties, Compr. Compos. Mater. (2000) 183–226, https://doi.org/10.1016/B0-08-042993-9/00074-7. Elsevier.
[47] A. Leliège, J. Grolleau, M. Allain, P. Blanchard, D. Demeter, T. Rousseau, J. Roncali, Small D-π-A systems with o -Phenylene-Bridged accepting units as active materials for organic photovoltaics, Chem. Eur J. 19 (2013) 9948–9960, https://doi.org/10.1002/chem.201301054.
[48] E. Ripaud, T. Rousseau, P. Leriche, J. Roncali, Unsymmetrical triphenylamine-oligothiophene hybrid conjugated systems as donor materials for high-voltage solution-processed organic solar cells, Adv. Energy Mater. 1 (2011) 540–545, https://doi.org/10.1002/aenm.201100065.
[49] Y. Kanemitsu, K. Suzuki, Y. Masumoto, Y. Tomiuchi, Y. Shiraishi, M. Kuroda, Optical properties of quasi-one-dimensional thiophene-based oligomers, Phys. Rev. B 50 (1994) 2301–2305, https://doi.org/10.1103/PhysRevB.50.2301.
[50] J. Kagan, S.K. Arora, Synthesis of .alpha.-thiophene oligomers via 1,3-butadiynes, J. Org. Chem. 48 (1983) 4317–4320, https://doi.org/10.1021/jo00171a032.
[51] R. Fitzner, E. Reinold, A. Mishra, E. Mena-Osteritz, H. Ziehlke, C. Körner, K. Leo, M. Riede, M. Weil, O. Tsaryova, A. Weiß, C. Uhrich, M. Pfeiffer, P. Bäuerle, Dicyanovinyl-Substituted oligothiophenes: structure-property relationships

and application in vacuum-processed small molecule organic solar cells, Adv. Funct. Mater. 21 (2011) 897–910, https://doi.org/10.1002/adfm.201001639.
[52] Y.N. Luponosov, D.O. Balakirev, I.V. Dyadishchev, A.N. Solodukhin, M.A. Obrezkova, E.A. Svidchenko, N.M. Surin, S.A. Ponomarenko, In search of efficient solubilizing groups for liquid and luminescent oligo(phenylene-thiophene) chromophores, J. Mater. Chem. C. 8 (2020) 17074–17082, https://doi.org/10.1039/D0TC04536E.
[53] H. Meier, J. Gerold, D. Jacob, The effect of 2,2-dicyanovinyl groups as electron acceptors in push–pull substituted oligo(1,4-phenylenevinylene)s, Tetrahedron Lett. 44 (2003) 1915–1918, https://doi.org/10.1016/S0040-4039(03)00120-5.
[54] H. Meier, Conjugated oligomers with terminal donor–acceptor substitution, Angew. Chem. Int. Ed. 44 (2005) 2482–2506, https://doi.org/10.1002/anie.200461146.
[55] S.J. Strickler, R.A. Berg, Relationship between absorption intensity and fluorescence lifetime of molecules, J. Chem. Phys. 37 (1962) 814–822, https://doi.org/10.1063/1.1733166.
[56] J. Shi, L.E. Aguilar Suarez, S.-J. Yoon, S. Varghese, C. Serpa, S.Y. Park, L. Lüer, D. Roca-Sanjuán, B. Milián-Medina, J. Gierschner, Solid state luminescence enhancement in π-conjugated materials: unraveling the mechanism beyond the framework of AIE/AIEE, J. Phys. Chem. C 121 (2017) 23166–23183, https://doi.org/10.1021/acs.jpcc.7b08060.
[57] D.O. Balakirev, Y.N. Luponosov, A.L. Mannanov, P.S. Savchenko, Y. Minenkov, D.Y. Paraschuk, S.A. Ponomarenko, Star-shaped benzotriindole-based donor-acceptor molecules: synthesis, properties and application in bulk heterojunction and single-material organic solar cells, Dye. Pigment. 181 (2020) 108523, https://doi.org/10.1016/j.dyepig.2020.108523.
[58] A. Köhler, H. Bässler, Electronic Processes in Organic Semiconductors, Wiley-VCH Verlag GmbH & Co. KGaA, Weinheim, Germany, 2015, https://doi.org/10.1002/9783527685172.
[59] Y. Wang, Y. Liu, S. Cao, J. Wang, A review on solution-processed perovskite/organic hybrid photodetectors, J. Mater. Chem. C 9 (2021) 5302, https://doi.org/10.1039/D1TC00643F.
[60] D. Yang, D. Ma, Development of organic semiconductor photodetectors: from mechanism to applications, Adv. Opt. Mater. 7 (2019) 1800522, https://doi.org/10.1002/adom.201800522.
[61] M. Skhunov, A.N. Solodukhin, P. Giannakou, L. Askew, Y.N. Luponosov, D.O. Balakirev, N.K. Kalinichenko, I.P. Marko, S.J. Sweeney, S.A. Ponomarenko, Pixelated full-colour small molecule semiconductor devices towards artificial retinas, J. Mater. Chem. C. 9 (2021) 5858–5867, https://doi.org/10.1039/D0TC05383J.
[62] P. Simón Marqués, J.M.A. Castán, B.A.L. Raul, G. Londi, I. Ramirez, M.S. Pshenichnikov, D. Beljonne, K. Walzer, M. Blais, M. Allain, C. Cabanetos, P. Blanchard, Triphenylamine/tetracyanobutadiene-based π-conjugated push–pull molecules end-capped with arene platforms: synthesis, photophysics, and photovoltaic response, Chem. Eur J. 26 (2020) 16422–16433, https://doi.org/10.1002/chem.202002810.
[63] O.V. Kozlov, X. Liu, Y.N. Luponosov, A.N. Solodukhin, V.Y. Toropynina, J. Min, M.I. Buzin, S.M. Peregudova, C.J. Brabec, S.A. Ponomarenko, M.S. Pshenichnikov, Triphenylamine-based push–pull molecule for photovoltaic applications: from synthesis to ultrafast device photophysics, J. Phys. Chem. C 121 (2017) 6424–6435, https://doi.org/10.1021/acs.jpcc.6b12068.
[64] E. Salamatova, O.V. Kozlov, Y.N. Luponosov, A.N. Solodukhin, V.Y. Toropynina, S.A. Ponomarenko, M.S. Pshenichnikov, Visualization of molecular excitons diffusion, in: A.A. Bakulin, R. Lovrincic, N. Banerji (Eds.), 2016, p. 99230K, https://doi.org/10.1117/12.2237620.
[65] B.A.L. Raul, Y.N. Luponosov, W. Yang, N.M. Surin, O. Douhéret, J. Min, T.L.C. Jansen, S.A. Ponomarenko, M.S. Pshenichnikov, Excited state dynamics and exciton diffusion in triphenylamine/dicyanovinyl push–pull small molecule for organic optoelectronics, Sci. Rep. 10 (2020) 21198, https://doi.org/10.1038/s41598-020-78197-2.
[66] O.V. Kozlov, Y.N. Luponosov, A.N. Solodukhin, B. Flament, Y. Olivier, R. Lazzaroni, J. Cornil, S.A. Ponomarenko, M.S. Pshenichnikov, Ultrafast exciton-to-polaron conversion in densely packed small organic semiconducting molecules, Adv. Opt. Mater. 5 (2017) 1700024, https://doi.org/10.1002/adom.201700024.
[67] H. Cha, Y. Zheng, Y. Dong, H.H. Lee, J. Wu, H. Bristow, J. Zhang, H.K.H. Lee, W.C. Tsoi, A.A. Bakulin, I. McCulloch, J.R. Durrant, Exciton and charge carrier dynamics in highly crystalline PTQ10:IDIC organic solar cells, Adv. Energy Mater. 10 (2020) 2001149, https://doi.org/10.1002/aenm.202001149.
[68] X. Liu, Y. Yan, A. Honarfar, Y. Yao, K. Zheng, Z. Liang, Unveiling excitonic dynamics in high-efficiency nonfullerene organic solar cells to direct morphological optimization for suppressing charge recombination, Adv. Sci. 6 (2019) 1802103, https://doi.org/10.1002/advs.201802103.
[69] Y. Terao, H. Sasabe, C. Adachi, Correlation of hole mobility, exciton diffusion length, and solar cell characteristics in phthalocyanine/fullerene organic solar cells, Appl. Phys. Lett. 90 (2007) 103515, https://doi.org/10.1063/1.2711525.
[70] G. Wei, R.R. Lunt, K. Sun, S. Wang, M.E. Thompson, S.R. Forrest, Efficient, ordered bulk heterojunction nanocrystalline solar cells by annealing of ultrathin squaraine thin films, Nano Lett. 10 (2010) 3555–3559, https://doi.org/10.1021/nl1018194.
[71] Y. Long, G.J. Hedley, A. Ruseckas, M. Chowdhury, T. Roland, L.A. Serrano, G. Cooke, I.D.W. Samuel, Effect of annealing on exciton diffusion in a high performance small molecule organic photovoltaic material, ACS Appl. Mater. Interfaces 9 (2017) 14945–14952, https://doi.org/10.1021/acsami.6b16487.
[72] Y. Zhang, M.T. Sajjad, O. Blaszczyk, A.J. Parnell, A. Ruseckas, L.A. Serrano, G. Cooke, I.D.W. Samuel, Large crystalline domains and an enhanced exciton diffusion length enable efficient organic solar cells, Chem. Mater. 31 (2019) 6548–6557, https://doi.org/10.1021/acs.chemmater.8b05293.
[73] O.V. Mikhnenko, P.W.M. Blom, T.-Q. Nguyen, Exciton diffusion in organic semiconductors, Energy Environ. Sci. 8 (2015) 1867–1888, https://doi.org/10.1039/C5EE00925A.
[74] S.M. Tuladhar, D. Poplavskyy, S.A. Choulis, J.R. Durrant, D.D.C. Bradley, J. Nelson, Ambipolar charge transport in films of methanofullerene and poly(phenylenevinylene)/methanofullerene blends, Adv. Funct. Mater. 15 (2005) 1171–1182, https://doi.org/10.1002/adfm.200400337.